This is an *Accepted Manuscript*, which has been through the Royal Society of Chemistry peer review process and has been accepted for publication.

*Accepted Manuscripts* are published online shortly after acceptance, before technical editing, formatting and proof reading. Using this free service, authors can make their results available to the community, in citable form, before we publish the edited article. We will replace this *Accepted Manuscript* with the edited and formatted *Advance Article* as soon as it is available.

You can find more information about *Accepted Manuscripts* in the **Information for Authors**.

# Journal Name

## ARTICLE

## Computational, Electrochemical, and Spectroscopic Studies of two Mononuclear Cobaloximes: The influence of an axial pyridine and solvent on the redox behaviour and evidence for pyridine coordination to cobalt(I) and cobalt(II) metal centres

Mark A. W. Lawrence,[a] Michael J. Celestine,[a] Edward T. Artis,[a] Lorne S. Joseph,[b] Deisy L. Esquivel,[c] Abram J. Ledbetter,[d] Donald M. Cropek,[e] William L. Jarrett,[f] Craig A. Bayse,[a] Matthew I. Brewer,[a] and Alvin A. Holder*[a]

$[Co(dmgBF_2)_2(H_2O)_2]$ **1** (where $dmgBF_2$ = difluoroboryldimethylglyoximato) was used to synthesize $[Co(dmgBF_2)_2(H_2O)(py)] \cdot 0.5(CH_3)_2CO$ **2** (where py = pyridine) in acetone. The formulation of complex **2** was confirmed by elemental analysis, high resolution MS, and various spectroscopic techniques. The complex $[Co(dmgBF_2)_2(solv)(py)]$ (where solv = solvent) was readily formed *in situ* upon the addition of pyridine to complex **1**. A spectrophotometric titration involving complex **1** and pyridine proved the formation of such a species, with formation constants, log $K$ = 5.5, 5.1, 5.0, 4.4, and 3.1 in 2-butanone, dichloromethane, acetone, 1,2-difluorobenzene/acetone (4:1, v/v), and acetonitrile, respectively, at 20 $^{o}$C. In strongly coordinating solvents, such as acetonitrile, the lower magnitude of $K$ along with cyclic voltammetry, NMR, and UV-visible spectroscopic measurements indicated extensive dissociation of the axial pyridine. In strongly coordinating solvents, $[Co(dmgBF_2)_2(solv)(py)]$ can only be distinguished from $[Co(dmgBF_2)_2(solv)_2]$ upon addition of an excess of pyridine, however, in weakly coordinating solvents the distinctions were apparent without the need for excess pyridine. The coordination of pyridine to the cobalt(II) centre diminished the peak current at the $E_{pc}$ value of the $Co^{I/0}$ redox couple, which was indicative of the relative position of the reaction equilibrium. Herein we report the first experimental and theoretical $^{59}Co$ NMR spectroscopic data for the formation of Co(I) species of reduced cobaloximes in the presence and absence of py (and its derivatives) in $CD_3CN$. From spectroelectrochemical studies, it was found that pyridine coordination to a cobalt(I) metal centre is more favourable than coordination to a cobalt(II) metal centre as evident by the larger formation constant, log $K$ = 4.6 versus 3.1, respectively, in acetonitrile at 20 $^{o}$C. The electrosynthesis of hydrogen by complexes **1** and **2** in various solvents demonstrated the dramatic effects of the axial ligand and the solvent on the turnover number of the respective catalyst.

## Introduction

The production and use of clean, renewable and high-energy-density sources are growing in demand to circumvent the use of fossil fuels, thus reducing the effects of carbon dioxide emissions and global warming. Hydrogen has been suggested as the leading candidate[1-4] and its production through the reduction of water appears to be a convenient solution for long-term storage and accessibility. Traditionally, noble metals of the platinum group metal series have been employed as catalytic centres in hydrogen production;[5-9] however, the high cost associated with these metals has led to searches for viable catalysts based on cheap and abundant first-row transition metals, such as nickel and cobalt.[10-14] Cobaloximes essentially mimic the active centre of hydrogenases[15, 16] and are a promising class of compounds for the production of hydrogen in acidic media.[17-19]

In addition to cobaloximes,[20-24] numerous cobalt-containing complexes exist for the catalytic reduction of protons to produce hydrogen. These include cobalt porphyrin derivatives,[25] macrocyclic complexes of [14]diene-N$_4$[26] and [14]tetraene-N$_4$[27] (tetraazamacrocycles), imine/oximes,[28] polypyridyl compounds,[29-33] bis(iminopyridine),[34] phosphine coordinated complexes,[35] and dithiolene (dithiolate)-containing[36] complexes (Figure 1), however, cobaloximes still

$^{a.}$Department of Chemistry and Biochemistry, Old Dominion University, Norfolk, VA 23529, U.S.A.
$^{b.}$University of the Virgin Islands, #2 John Brewers Bay, Charlotte Amalie, VI 00802, U.S.A.
$^{c.}$Johnson C. Smith University, 100 Beatties Ford Road, Charlotte, NC 28216, U.S.A.
$^{d.}$University of Michigan, Applied Physics, Ann Arbor, MI 48108, U.S.A.
$^{e.}$U.S. Army Corps of Engineers, Construction Engineering Research Laboratory, Champaign, IL 61822, U.S.A.
$^{f.}$School of Polymers and High-Performance Materials, The University
$^{g.}$of Southern Mississippi, 118 College Drive, #5050, Hattiesburg,
$^{h.}$MS 39406-0076, U.S.A.
† Alvin A. Holder. E-mail: aholder@odu.edu;  fax: 757-683-4628.
Electronic Supplementary Information (ESI) available: [details of any supplementary information available should be included here]. See DOI: 10.1039/x0xx00000x

continue to generate a lot of interest due to their high activity towards electrocatalytic proton reduction.[15, 19, 37-39]
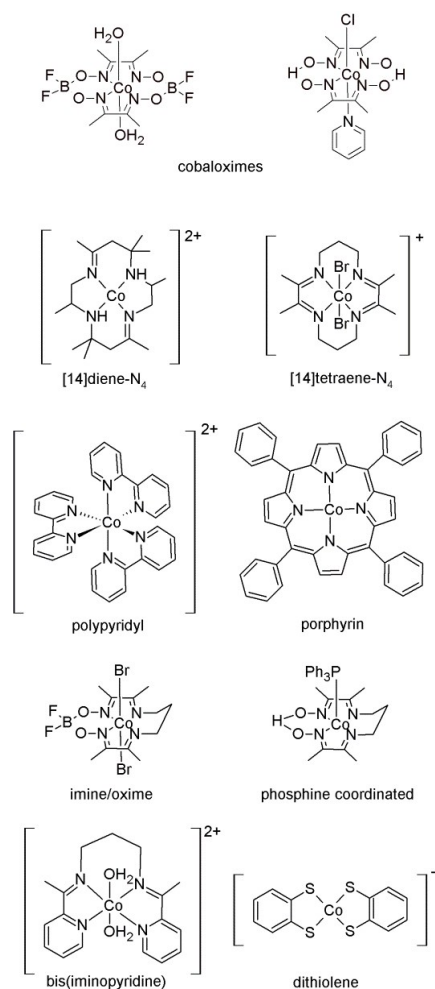


Figure 1. Examples of some cobalt-containing complexes employed in the electrocatalytic reduction of protons.

The most plausible route in the catalytic evolution of hydrogen involves the formation of a Co(I) species from either a Co(III) or Co(II) precursor.[11, 36] Recent studies have been geared towards studying the Co(I) intermediate through NMR spectroscopy,[40] X-ray absorption spectroscopy (XAS),[41] and high frequency electron paramagnetic resonance (HFEPR)[42] techniques. Other studies[19, 36, 37] have employed bridging binuclear systems to understand and enhance the catalyst performance for hydrogen production. For photocatalytic processes employing molecular systems with a pyridine-type linker from the photoactive centre to a cobaloxime catalytic centre,[43-45] the effect of a bridging ligand in the axial position on the electron transfer relative to the cobaloxime alone in a particular solvent has not been studied for the BF$_2$ capped cobaloxime species. In photocatalytic experiments, acid sources such as *p*-cyanoanilinium, anilinium, and triethylammonium cations are employed.[28]

Ligand dissociation is a common occurrence in catalytic processes. An understanding of the ligand dissociation and the

electron transfer kinetics has been arrived at from radiolytic studies carried out on some cobalt(III) complexes, for example, [Co(dmgH)$_2$(py)(Cl)] (where dmgH = dimethylglyoximato).[29, 46, 47] Radiolytic and high-pressure kinetic studies of cobalt(III) compounds such as [Co(NH$_3$)$_5$(CH$_3$)]$^{2+}$ and [Co(phendione)$_2$Cl$_2$]Cl (where phendione = 1,10-phenanthroline-5,6-dione), directed towards the lability of the ligands on the resulting Co(II) species,[48-50] and other studies involving Co(II)[51] and Co(III)[47, 49] complexes bearing polypyridyl ligands such as [Co(pic)$_2$(bpy)], [Co(bpy)$_3$]$^{3+}$, [Co(phen)$_3$]$^{3+}$, [Co(en)$_2$(bpy)]$^{3+}$, and [Co(en)$_2$(phen)]$^{3+}$, (where pic = 2-picolinato, bpy = 2,2'-bipyridine, phen= 1,10-phenanthroline, and en = ethylenediamine) show the formation of a ligand radical anion species, which decays by either protonation of the ligand,[52, 53] or by reduction of the metal centre via intramolecular electron transfer. Kumar and co-workers[50] have attempted to distinguish between [Co$^I$(dmgBF$_2$)$_2$(H$_2$O)]$^-$ species and the pyridine coordinated species. In their work, radiolysis and chemical means of reduction in MeOH/H$_2$O, were presented as evidence of the various oxidation states of cobalt. However, in their report, the effect of solvent on the coordination of pyridine to the Co(II) state was not investigated. In that study, they also showed that both the pyridine and chloride axial ligands dissociate from the Co(II) species of [Co(dmgH)$_2$(py)(Cl)]. These studies are of interest, because the stability of the different oxidation states of the cobaloxime and its coordination sphere are believed to have a significant effect on its catalytic properties. In strongly coordinating solvents (as determined from solvent exchange rate constants[54, 55] for example), or in the presence of various nucleophiles, the axial ligands of the cobaloxime may be easily substituted,[41, 56] which is expected to influence the redox and substitution chemistries of the cobalt centre. Acetonitrile has proven to be a very convenient solvent for the electrocatalytic and photocatalytic studies of cobaloximes, however a study of the ability and influence of this solvent (and other coordinating solvents) to effectively compete with the complexation of the axial ligand has been neglected, and to the best of our knowledge, such a study has not been reported in the literature.

Various electrocatalytic studies on proton reduction using cobalt species[11, 15, 27, 34, 37, 40, 57, 58] have focused on the variation of the equatorial ligands. Substitution at the backbone of the equatorial glyoxime ligands significantly affects the electrochemical potentials of the Co$^{II/I}$ redox couple, and also affects the proton reduction electroactivity on the cyclic voltammetry time scale.[59] Similar effects are observed when the hydrogen-bonding protons between the equatorial ligands are substituted with BF$_2$.[59, 60] Cobaloximes of the type [Co(dmgH)$_2$(L)Cl] (where L = a nitrogen-containing Lewis base such as pyridine and its derivatives) have been studied to explore the influence of the axial ligand on the electroactivity of the cobaloxime.[39, 59] However, in the case of the BF$_2$ capped system [Co(dmgBF$_2$)(solv)$_2$] (where solv = a solvent molecule such as MeOH, H$_2$O, etc.), the lability of the axial position of the Co(II) metal centre has resulted in an elusive species with pyridine in the axial position, and as such, this species has

been primarily studied as a species generated *in situ*.[22, 61] Owing to this, there is a lack of data that correlates the electroactivity of the $[Co(dmgBF_2)_2(solv)_2]$ species to its $[Co(dmgH)_2(L)Cl]$ analogue with regards to an axial pyridine. These data are critical as one of the most practical approaches of transitioning cobaloximes to potentially useful applications involves coupling a cobalt(II) metal centre to a photosensitizer such a ruthenium(II) metal centre with the aid of a bridging ligand. In these systems, para-substituted pyridine linkers have been employed as important templates in the syntheses of photocatalytic systems reported for the reduction of protons to form hydrogen.[44, 62, 63]

For many years, we have been interested in the development of transition metal complexes that contain at least one cobalt metal centre,[44, 64-71] and also inorganic reaction mechanisms that involve electron transfer processes.[64, 65, 72-74] Recently,[44] we reported the synthesis, characterization, and photocatalytic studies of novel mixed-metal binuclear ruthenium(II)–cobalt(II) photocatalysts $[Ru(pbt)_2(L-pyr)Co(dmgBF_2)_2(H_2O)](PF_6)_2$ (where pbt = 2-(2′-pyridyl)benzothiazole, L-pyr = (4-pyridine)oxazolo[4,5-*f*]phenanthroline), $[Ru(Me_2bpy)_2(L-pyr)Co(dmgBF_2)_2(OH_2)](PF_6)_2$ (where $Me_2bpy$ = 4,4′-dimethyl-2,2′-bipyridine), and $[Ru(phen)_2(L-pyr)Co(dmgBF_2)_2(OH_2)](PF_6)_2$ for hydrogen evolution in acidic acetonitrile. Photocatalytic studies carried out in acidified acetonitrile demonstrated constant hydrogen generation longer than a 42 hour period as detected by gas chromatography. Time resolved spectroscopic measurements on $[Ru(pbt)_2(L-pyr)Co(dmgBF_2)_2(H_2O)](PF_6)_2$, proved an intramolecular electron transfer from an excited Ru(II) metal centre to the Co(II) metal centre via the bridging L-pyr ligand. This resulted in the formation of a cobalt(I)-containing species that was essential for the production of $H_2$ gas in the presence of $H^+$ ions. Based on the fact that we are very interested in mechanistic studies on the role of the cobalt(I) metal centre during the course of the production of hydrogen in the solvent media, we have embarked upon a detailed study of the solution chemistry of Co(II) and Co(I) metal centres within cobaloximes to assist us in this effort. As such, this study reports the isolation and characterization of a new cobaloxime, complex **2** (Figure 2) which contains the elusive pyridine in the axial position of the cobaloxime, together with electrochemical and spectroelectrochemical studies in both strongly and weakly coordinating solvents to assess the effect of solvent on the extent of coordination of the pyridine in the axial position to complex **1**, and how this influences the cobaloxime's reactivity in the production of hydrogen. We also wish to determine the extent and the effect of pyridine's coordination on the Co(I) metal centre in the respective solution, with the aid of UV-visible, $^{11}B$, $^{19}F$, and $^{59}Co$ NMR spectroscopies and density functional theory (DFT) calculations. Complex **2** serves a dual role in which it will allow for a(n) (indirect) comparison to the $[Co(dmgH)_2(L)Cl]$ species, and simultaneously act as a model for the para-substituted pyridine linkers employed in photocatalytic systems employing complex **1** as the catalytic site. This is a critical step to understand the electron transfer process and the stability of a

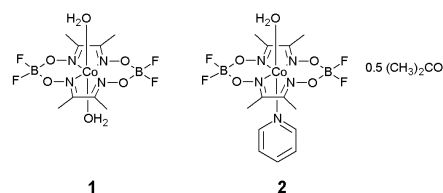pyridine-Co(I) species that is likely to be formed in reduced cobaloximes.



Figure 2. Structures of complexes $[Co(dmgBF_2)_2(H_2O)_2]$ (complex **1**) and $[Co(dmgBF_2)_2(H_2O)(py)]•0.5(CH_3)_2CO$ (complex **2**).

## Results and Discussion

### Characterizations and equilibrium studies

Complex **1** was reacted with 1.4 equivalents of pyridine in acetone to produce $[Co(dmgBF_2)_2(H_2O)(py)]•0.5(CH_3)_2CO$ **2** (see Scheme 1). The formulation of complex **2** is supported by the $M^+$ parent ion observed in the High Resolution Mass Spectrum (HRMS), the elemental analysis, as well as the other spectroscopic characterizations (see ESI, Figure S1-S4[†]). In the FTIR spectrum, there are distinct shifts (see ESI, Figure S2[†]) in the C=N, N-O, and B-F stretching frequencies of complex **1** compared to complex **2**, as well as two peaks at 690 and 758 $cm^{-1}$ all consistent with the coordination of pyridine to the cobalt centre.[75] Additionally, the magnetic moment $\mu_{eff}$ = 1.28 ± 0.02 B.M. for complex **2** (at ambient temperature) is consistent with low spin Co(II). Both complexes **1** and **2** are reasonably soluble in acetonitrile, acetone, butanone, but moderately soluble in water; while they are soluble at <0.1 mM in 1,2-difluorobenzene. $[Co(dmgBF_2)_2(H_2O)_2]$ is known to have an enhanced solubility in acetone relative to alcohols.[55] Acetone generally behaves as a polar weakly coordinating solvent, and this nature was evident from the synthetic protocol of complex **2**, where the axial water molecule is retained in the solid as shown in the mass spectrum. The UV-visible spectra of both complexes in various solvents are given in the ESI (see Figures S3 and S4) and the molar extinction coefficients are shown in Table 1.
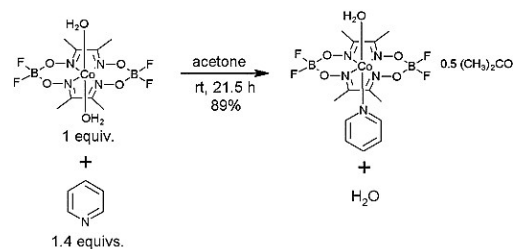


Scheme 1. Synthesis of complex **2**.

In the UV-visible portion of the spectrum, the band between 420 and 450 nm showed the most variation between the complexes. In weakly coordinating solvents (acetone, 2-butanone, etc.), this band is observed at ca 450 nm for complex **1** and at ca 430 nm for complex **2**. For complex **2**, the tail and the band which goes into the NIR region are also more

pronounced. These changes can be interpreted as additional evidence for the coordination of pyridine to the Co(II) complex in the solution state. This band in the NIR region is characteristic of, and also confirmed, the low spin nature of the cobalt(II) metal centre in both species.[44]

Table 1. The absorption maxima (nm) and molar extinction coefficients ($M^{-1}$ $cm^{-1}$) of complexes **1** and **2**.

| solvent | complex | $\lambda_1$ ($10^{-3} \varepsilon$) | $\lambda_2$ ($10^{-3} \varepsilon$) | $\lambda_3$ ($10^{-2} \varepsilon$) |
|---------|---------|------------|------------|------------|
| acetonitrile | **1** | 323 sh (2.5) | 425 (3.6) | 1162 (1.1) |
| water | **1** | -- | 455 (2.7) | -- |
| acetone | **1** | -- | 446 (2.7) | 1294 (0.7) |
| 2-butanone | **1** | -- | 449 (2.9) | 1319 (0.6) |
| 1,2-difluorobenzene: acetone (4:1, v/v) | **1** | -- | 444 (2.7) | 1170 (1.3) |
| acetonitrile | **2** | 323 sh (4.1) | 425 (4.8) | 1144 (1.5) |
| water | **2** | -- | 454 (3.2) | -- |
| acetone | **2** | -- | 436 (2.8) | 1135 (2.7) |
| 2-butanone | **2** | -- | 431 (2.6) | 1131 (2.7) |
| 1,2-difluorobenzene: acetone (4:1, v/v) | **2** | -- | 420 (3.9) | 1138 (2.6) |

The complex, $[Co(dmgBF_2)_2(H_2O)_2]$ has a very rapid solvent exchange rate that is comparable to the hexasolvated high-spin Co(II) species.[54, 55] Thus, it is expected that the axial water ligand(s) are substituted with coordinating solvents. The pyridine coordinated species can also be generated *in situ*. In weakly coordinating solvents (see ESI, Figures S5-S7[†]), the addition of pyridine to complex **1** caused a blue shift from 450 nm to 430 nm which coincides with the band observed in the ketone solutions of complex **2**. In the NIR region, there was an increase in the intensity of the absorbance coupled with a blue shift in $\lambda_{max}$ in going from complex **1** to complex **2**. In acetonitrile (see Figure 3), this transformation is best observed in the NIR region as the changes in the UV region are masked by an excess of pyridine. In water (not shown), the changes in the UV-visible region of the spectrum of complex **1** upon the addition of pyridine are difficult to interpret. In an unbuffered environment, there is the possibility of deprotonating the axial water molecule at higher pH values (induced by the addition of pyridine). Additionally, it was observed that the complex interacts with all the buffer systems we have tried which limited our ability to interpret the changes at higher ratios of pyridine to complex. The poor solubility of the complexes in water prevents the acquisition of reasonable spectral data in the NIR region. The observations made in the non-aqueous solvents point to the formation of complex **2** from complex **1** *in situ* upon the addition of pyridine. Using these spectral transformations, the stoichiometry of the interaction between pyridine and complex **1** in acetonitrile (and other solvents) was determined from mole ratio plots (see ESI, Figures S8–S17) and was found to be 1:1 (Eq. 1, where solv = solvent molecule) with up to five times excess pyridine.

$$[Co(dmgBF_2)_2(solv)_2] + py \underset{}{\overset{K_1}{\rightleftharpoons}} [Co(dmgBF_2)_2(solv)(py)] + solv \quad (1)$$
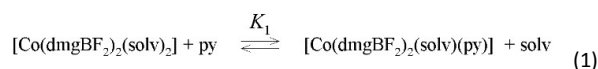
From these data, the formation constant[22, 76] for the monopyridine species (complex **2**) from complex **1** was determined (see Table 2 and the experimental section for details on how these values were determined). In all the solvents explored, the mole ratio and log plots also indicate that the monopyridine species is the major species over the concentration range studied (see ESI Figures S8–S17). The stoichiometry and equilibrium constants are consistent with analogous systems reported by Nonaka and Hamada.[22] In water, and other coordinating solvents, the equilibrium between $[Co(dmgBF_2)_2(solv)_2]$ or $[Co(dmgH)_2(solv)_2]$ and pyridine (and analogous Lewis bases) has been found to be relatively small and the propensity to form a stoichiometry greater than 1:1 is even smaller.[22, 50, 61] From the magnitude of the equilibrium constant in acetonitrile ($1.3 \times 10^3$ at 20 $^{o}$C), it can be easily deduced that the dissociation of the pyridine from $[Co(dmgBF_2)_2(CH_3CN)(py)]$ is significant at 20 $^{o}$C. This dissociation, which can occur with the pyridine linker systems employed in bridging binuclear systems, has been largely ignored in the interpretation of data presented in the literature. In the case of acetone and 2-butanone, there are much larger formation constants for the monopyridine complex (complex **2**) compared to acetonitrile and represent suitable solvents for studying complex **2**.

Table 2. Formation constants for some pyridine coordinated Co(II) oxime complexes at 20 ± 1 $^{o}$C.

| Co(II) precursor | solvent | log $K_1$ | Ref. |
|------------------|---------|-----------|------|
| $[Co(dmgBF_2)_2(H_2O)_2]$ | 2-butanone | 5.5 | This work |
| $[Co(dmgBF_2)_2(H_2O)_2]$ | acetone | 5.0 | This work |
| $[Co(dmgBF_2)_2(H_2O)_2]$ | dichloromethane | 5.1 | This work |
| $[Co(dmgBF_2)_2(H_2O)_2]$ | 1,2-difluorobenzene/acetone (4:1, v/v) | 4.4 | This work |
| $[Co(dmgBF_2)_2(H_2O)_2]$ | acetonitrile | 3.1 | This work |
| $[Co(dmgBF_2)_2(H_2O)_2]$ | DMF | 2.3* | 22 |
| $[Co(dmgH)_2(H_2O)_2]$ | methanol | 2.1 | 61 |
| $[Co(dpgBF_2)_2(H_2O)_2]$ | DMF | 4.2* | 22 |
| $[Co(dpgH)_2(H_2O)_2]$ | DMF | 2.9* | 22 |

* At 25 $^{o}$C
dpgH = diphenylglyoximato
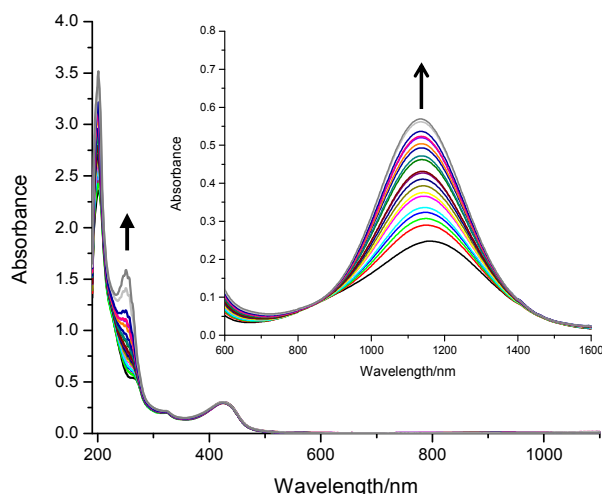dpgBF$_2$ = difluoroboryldimethylglyoximato

Figure 3. Spectrophotometric titration of complex **1** with pyridine in acetonitrile. [complex **1**] = 0.1 mM, NIR region shown in inset ([complex **1**] = 2 mM), path length = 1 cm. Arrow represents increasing [pyridine], see Table S1.

### Electrochemical and chemical reduction studies

In acetonitrile, on oxidatively or reductively initiated scans, the cyclic voltammograms of complexes **1** and **2** (Figure 4) showed a quasi-reversible wave for the Co[III/II] redox couple, reversible waves corresponding to the Co[II/I] redox couple,[44] as well as quasi-reversible waves corresponding to the Co[I/0] redox couple and the reduction of the ligand (most likely reduction of the C=N bonds). The behaviour (Scheme 2) of the cobalt(II) centre is comparable to what has been reported for complex **1** in the literature.[27, 77]
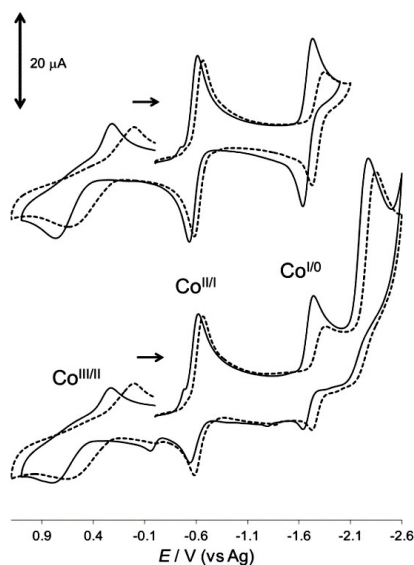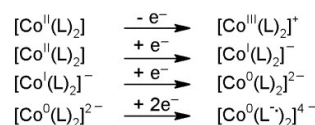


Figure 4. A comparison of the cyclic voltammograms of complexes **1** and **2** in acetonitrile on a glassy carbon working electrode versus Ag quasi-reference electrode. [complex **1**] = 1.04 mM (solid lines) and [complex **2**] = 1.02 mM (broken lines), supporting electrolyte = 0.10 M [$^n$Bu$_4$N]ClO$_4$, and scan rate = 100 mV s$^{-1}$. The effect of the scan range on the shapes of cobalt peaks is shown above.



Scheme 2. Summary of the redox behaviour in acetonitrile where L = dmgBF$_2$. Solvent excluded for simplicity.

The equilibrium established in strongly coordinating solvents, as described above, between complex **1** and complex **2** results in the profile of the cyclic voltammograms of both species being very similar in acetonitrile as shown in Figure 4. In acetone and 2-butanone where complex **2** has a much larger formation/stability constant, the cyclic voltammograms for complex **1** can be clearly distinguished from complex **2** via the absence of the cathodic peak in the region of the Co[I/0] redox couple for complex **2** (as shown in Figure 5a and Figure S22). The addition of five equivalences of pyridine to complex **1**, in any of the solvents studied, as discussed above, shifts the equilibrium towards the monopyridine species (complex **2**), and the Co[I/0] redox couple is not observed. It is most likely that the suppression of this cathodic wave (see Figure 5b) is related to the coordination of the pyridine to the Co(II), in which it affects the Co[I/0] redox couple. The addition of sterically encumbering pyridines (2-methylpyridine and 2,6-dimethylpyridine) up to fifteen equivalences to an acetonitrile solution of complex **1** did not affect peak potentials in the cyclic voltammogram (see ESI, Figure S26-27†). The inability of these sterically hindered substituted pyridines to coordinate was also observed for the [Co(dmgH)$_2$(H$_2$O)$_2$] system,[39] and indicated that the change(s) observed in the cyclic voltammogram of complex **1** in the presence of pyridine is not the result of Brønsted acid-base behaviour. On the other hand, the addition of 4-aminopyridine resulted in similar changes to what was observed with the addition of pyridine and further validates the use of cyclic voltammetry to assess the coordination of pyridine. Interestingly, in the weakly coordinating solvents, where the integrity of complex **2** is retained, the addition of an excess (five equivalences) of pyridine did not: (i) result in an enhancement of the peak currents, (ii) cause any shift in the peak potentials, or (iii) result in the appearance of any additional peaks in the cyclic or square wave voltammograms (not shown) of complex **2**. This points to the dominance of the monopyridine species over these concentration ranges. The values of the reduction potentials are summarized in Table 3 for comparative purposes. To the best of our knowledge, this is the first time that a cobaloxime is being studied by cyclic voltammetry in either ketone solvents or 1,2-difluorobenzene. Similar to the UV-visible measurements, cyclic voltammetry is a valuable technique to illustrate the effect of the solvent coordinating ability on the extent of the pyridine substitution.

In acetonitrile where an excess of pyridine is added to force the formation of complex **2** (Table 3, entry 3), only the potentials for the cobalt couples are affected, but not the potential for the dmgBF$_2^-$ ligand. Using the potential of the ligand as reference, it is fair to assume that the addition of the

pyridine can affect the electrochemical properties of the cobalt(II) metal centre. In the other solvent systems, where complex **2** is stable without excess pyridine, similar conclusions can be deduced. Generally, the potential for the $Co^{III/II}$ and $Co^{II/I}$ redox couples are shifted towards zero (vs Ag) in complex **2** compared to complex **1**, and suggests that the addition of pyridine makes the complex more accessible to oxidation and reduction processes. From these findings, we have clearly shown that cyclic voltammetry can be used to qualitatively assess the coordination of pyridine to the Co(II) metal centre in the $BF_2$ capped cobaloxime.
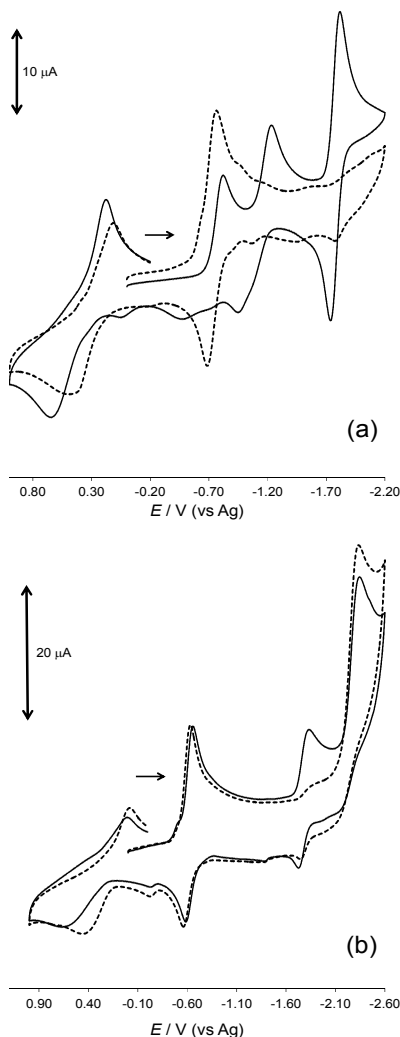
(a)

(b)

Figure 5. Cyclic voltammograms of complexes **1** and **2** on a glassy carbon working electrode versus Ag quasi-reference electrode, supporting electrolyte = 0.10 M [$^nBu_4N$]ClO$_4$, and scan rate = 100 mV s$^{-1}$. (a) In acetone, [complex **1**] = 1.12 mM (solid lines) and [complex **2**] = 1.04 mM (broken lines) and (b) in acetonitrile, [complex **2**] = 1.02 mM (solid lines) and [complex **2**] = 1.02 mM with 5.09 mM pyridine (broken lines).

Table 3. The reduction potentials of complexes **1** and **2** at a glassy carbon working electrode versus Ag.

| Entry | Species | Solvent | $Co^{III/II}$ / V | $Co^{II/I}$ / V | $Co^{I/0}$ / V | dmgBF$_2$ $^{0/-}$ / V |
|---|---|---|---|---|---|---|
| 1 | **1** | acetonitrile | +0.70 | −0.58 | −1.69 | −2.21 |
| 2 | **2** | acetonitrile | +0.60 | −0.63 | −1.77 | −2.30 |
| 3 | **2**‡ | acetonitrile | +0.46 | −0.60 | -- | −2.30 |
| 4 | **1** | acetone | +0.65 | −0.82 | −1.20 | −1.79 |
| 5 | **2** | acetone | +0.50 | −0.73 | -- | -- |
| 6 | **1** | water* | +0.48 | −0.60 | −0.85 | -- |
| 7 | **2** | water* | +0.31 | −0.50 | -- | -- |
| 8 | **1** | 2-butanone | +0.88 | −0.58 | −0.99 | −1.58 |
| 9 | **2** | 2-butanone | +0.64 | −0.66 | -- | -- |
| 10 | **1** | 1,2-difluorobenzene /acetone (4:1, v/v) | +0.36 | −0.82 | −1.20 | −1.82 |
| 11 | **2** | 1,2-difluorobenzene /acetone (4:1, v/v) | +0.38 | −0.80 | -- | -- |

‡ in five times excess pyridine, *values are versus AgCl/Ag. All the potentials quoted are determined from square wave voltammetry.

Pyridine is renowned for its electron donating ability and has been used to stabilize low oxidation states in pyridine-enhanced pre-catalyst preparation stabilization and initiation (PEPPSI) complexes.[78-81] In water, the $Co^{II/I}$ redox couple illustrated a quasi-reversible behaviour for complex **1**, but in the presence of excess pyridine the behaviour became reversible ($i_{pa}/i_{pc}$ = 0.97, see ESI, Figure S25 vs S21[†]). This behaviour in addition to the absence of the $Co^{I/0}$ cathodic wave is quite intriguing, and is also observed in the ketone solvents. The transition of the cyclic voltammogram in going from complex **1** to complex **2** is consistent in all the solvents used here (in terms of the absence of $Co^{I/0}$ redox couple in the cyclic voltammograms of complex **2**). Repetitive cycling did not result in the appearance of any new peaks in the cyclic voltammograms of complex **2**. It therefore appears that the coordination of the pyridine causes the reduction of $Co^{I/0}$ couple to become more negative than the potential window of the solvent, and thus inaccessible. This we attribute to the electron donating ability of the pyridine. This nature allows for the use of cyclic voltammetry in qualitatively identifying the coordination of pyridine to complex **1**.

It is unclear from the electrochemical studies if the pyridine has a dissociation/association equilibrium with the Co(I) metal centre as is established with the Co(II) state. Indeed, it has been suggested that the pyridine coordinates more strongly to the Co(I) metal centre than it does to the Co(II) metal centre in [Co(dmgH)$_2$(H$_2$O)$_2$] and [Co(dmgBF$_2$)$_2$(H$_2$O)$_2$].[50] Both complexes **1** and **2** were chemically reduced in acetonitrile under an argon atmosphere using tetrabutylammonium borohydride ([$^nBu_4N$]BH$_4$) (or powdered NaBH$_4$) as a reductant, and their spectra are given in Figure 6. The addition of [$^nBu_4N$]BH$_4$ resulted in an increase in the absorbance between 500 and 800 nm, which corresponded to the formation of a Co(I) species.[27, 50, 60, 74, 82]
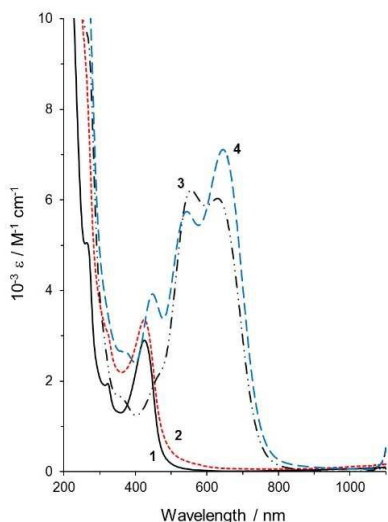
Figure 6. UV-visible spectra (acetonitrile solutions) of complex **1** (black, (solid, (1)), complex **2** (broken/red, (2)), complex **1** in excess [$^n$Bu$_4$N]BH$_4$ (black( – ··, (3)), complex **2** in excess [$^n$Bu$_4$N]BH$_4$ (blue, (– –, 4)).

Analogous Co(I) species of complex **1** such as [Co(dpgBF$_2$)$_2$(CH$_3$CN)]$^-$ (where dpgBF$_2$ = difluoroboryldiphenylglyoximato) as well as a cobaloxime containing a bis(imino)acenaphthene (BIAN) appended ligand and the pyridine coordinated anion of complex **2** have been isolated with a pentacoordinate geometry[27, 83, 84] corresponding to a loss of solvent from the axial position of the octahedral Co(II) starting material. It is evident that the differences between the UV-visible spectra of the reduced forms of complexes **1** and **2** are due to the presence of the pyridine in the axial position, in place of the solvent molecule, in the square planar pyramidal complex. These Co(I) species are very sensitive to oxygen and are unstable at low to moderate pH values (pH < 10) due to their interaction with H$^+$.[50] In our experiments, we found that if the reduced cobalt species (a Co(I) species) is oxidized upon exposed to air, the change is irreversible and the Co(I) species will not reform in an excess of the reducing agent under inert atmosphere. The exact nature of the species formed upon exposure to oxygen is unclear at this point.

The addition of pyridine to the Co(I) species in an acetonitrile solution of [Co(dmgBF$_2$)$_2$(CH$_3$CN)]$^-$ (which is believed to be formed by reducing complex **1** with excess of the BH$_4$$^-$ salt) caused spectral transformations that resemble those of a borohydride reduced solution of complex **2** (i.e., the proposed [Co(dmgBF$_2$)$_2$(py)]$^-$ species) as shown in Figure 7. It is quite clear that the sequential addition (titration) of the pyridine results in distinct changes to the spectra of the solution and provides evidence for the formation of a Co$^I$-pyridine coordination compound. The data also indicates that less than stoichiometric amounts of pyridine will cause significant transformation in the visible region of the spectrum (unlike the +2 oxidation state) in acetonitrile. The changes in

the absorbance values upon the addition of pyridine are also suggestive of an equilibrium between the "pyridine-bound" and the "free" Co(I) species in acetonitrile. From the mole ratio plot, the stoichiometry was found to be 1:1 (pyridine:complex), indicating the formation of a monopyridine species. Using the method of Nonaka and Hamada,[22] log $K$ = 4.6 for the Co(I) species as compared to 3.1 for the Co(II) species. The change in geometry and electronic configuration may be the sources of this large difference, despite the small difference in the reduction potentials observed for the Co$^{II/I}$ redox couple in acetonitrile (Table 3). Indeed, the crystal structure of the anion of complex **2**[83] reveals a shorter Co-N bond than for the corresponding Co(II) species[20] (1.83 vs 1.88 Å) and supports the larger formation constants obtained.
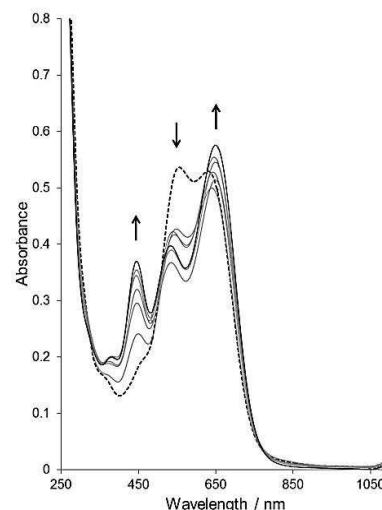


Figure 7. UV-visible spectra (acetonitrile solutions) of [$^n$Bu$_4$N]BH$_4$ reduced [complex **1**] = 1.0 mM (broken line), and [$^n$Bu$_4$N]BH$_4$ reduced complex **1** with various equivalences (0.50, 1.0, 1.5, 2.0, 2.5 and 4.0) of pyridine, path length = 1 mm. Arrows indicate the absorbance change with increasing [pyridine].

### Spectroelectrochemical studies

From cyclic voltammetric and chemical reduction studies, it is clear that the presence of pyridine within the coordination sphere influences the reduction of the cobalt(II) metal centre, as well as the spectrum of the Co(I) species. This difference is most pronounced in relatively weakly coordinating solvents. To provide further insight, and to justify our assignments for the Co$^{II/I}$ redox couple, as well as to verify that the spectra obtained in the presence of [$^n$Bu$_4$N]BH$_4$ is correctly assigned to a Co(I) species, studies of the spectral changes under cathodic potentials in the various solvents were performed. In acetonitrile (Figure 8), UV-visible spectral changes of complex **1** at a constant potential of −1.0 V versus Ag, resulted in spectral characteristics similar to the Co(I) species generated above and to that reported by Pantani et al.,[82] which was generated by electrochemical methods. Comparing the reduced spectra of complexes **1** and **2**, there are subtle differences. For complex **1**, the peak at ca 430 nm decreases in

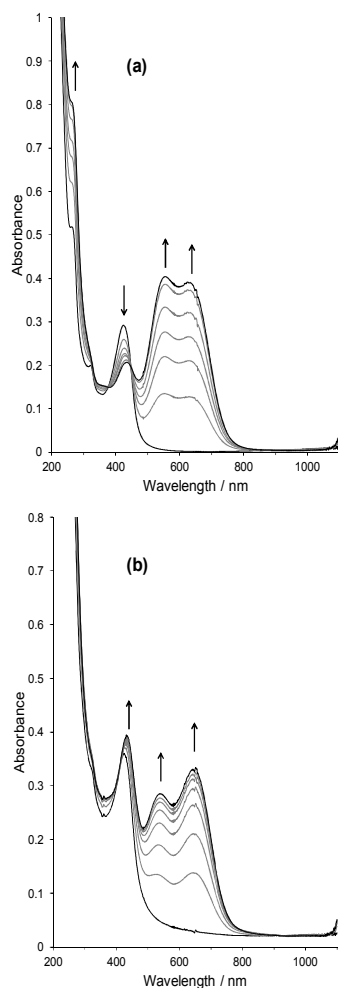absorbance upon reduction whereas in complex **2**, this absorbance increases.



Figure 8. Absorbance changes in the UV-visible spectra of complexes **1** and **2** in acetonitrile at a constant potential of −1.0 V versus Ag, supporting electrolyte = 0.10 M [$^n$Bu$_4$N]ClO$_4$, path length = 1 mm. (a) [complex **1**] = 1.05 mM and, (b) [complex **2**] = 1.02 mM.
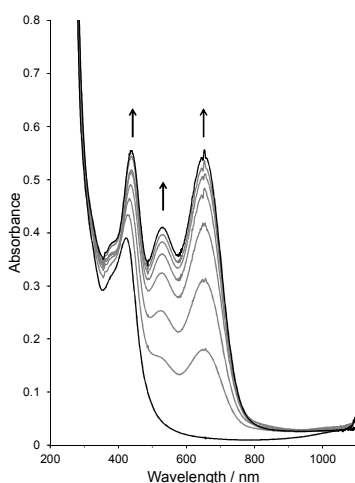


Figure 9. Absorbance changes in the UV-visible spectra of complex **2** with pyridine in acetonitrile at a constant potential of −1.0 V versus Ag, supporting electrolyte = 0.10 M [$^n$Bu$_4$N]ClO$_4$, path length = 1 mm. [complex **2**] = 1.02 mM and [pyridine] = 5.09 mM.

Additionally, the relative intensities of the peaks assigned to the formation of the Co(I) species at ca 550 and 640 nm differ between complexes **1** and **2**. The addition of excess pyridine to acetonitrile solutions of complexes **1** or **2** yields enhanced absorbance for the Co(I) state relative to a solution of only complex **2** (see Figure 9 and ESI Figures S31–S34[†] vs Figure 8b). This further confirms the speciation/dissociation in acetonitrile as given in Eq. 1. In water, only one broad band with $\lambda_{max}$ at 640 nm develops when complex **1** is reduced (see ESI, Figure S35[†]), which is consistent with the spectrum observed by Kumar et al.[50] In the presence of excess pyridine, similar features to the acetonitrile solution (i.e., the dual band for the Co(I) species) are observed (see ESI, Figure S36[†]), and here also our findings are consistent with the report of Kumar *et al.*[50] in aqueous media. In the weakly coordinating solvents, acetone, 2-butanone, and 1,2-difluorobenzene/acetone, the reduction of complex **1** at the Co$^{II/I}$ redox couple develops a similar band to that of water, but red shifted by ~100 nm, whereas complex **2** gave the same spectral features that were observed in acetonitrile (and water) (see ESI, Figures S37–S45[†]). Likewise with acetonitrile and water solutions, the reduction of complex **1** in the presence of excess pyridine resulted in the spectral characteristics of complex **2** under reduction. Interestingly, the addition of excess pyridine to the ketone solutions of complex **2** did not enhance the absorbance change upon reduction. This strongly supports the idea that the dissociation of complex **2** is insignificant in these solvents, and the monopyridine species is the predominant species. It is very important that the differences in the spectra of Co(I) species of complex **1** in these solvents are highlighted. In water and the ketone solvents, only a single band develops between 600 and 900 nm in the absence of pyridine, however, in acetonitrile, a dual band develops for Co(I) species of complex **1**. We suspect that the coordination of the nitrogen from the acetonitrile solvent causes the splitting of a band at approximately 600 nm (due to a Co(I) metal centre) in a manner similar to pyridine. This splitting may be the result of back bonding from the electron rich Co(I) to the sp$^2$ or sp hybridized nitrogen. This idea was also postulated by Espenson and co-workers on the basis of the short Co-N bond length.[83]

### $^{11}$B, $^{19}$F, and $^{59}$Co NMR spectroscopic studies

Transition metal NMR chemical shifts are useful probes of the structure and reactivity of many coordination complexes, since those chemical shifts are sensitive to tiny variations at the coordination metal centre under investigation.[85] We are interested in the coordination of pyridine, and its analogues, in the solution state as functional models for photocatalytic systems. Previously, we have used $^{11}$B, $^{19}$F, and $^{59}$Co NMR spectroscopic studies to verify coordination of a (4-pyridine)oxazolo[4,5-*f*]phenanthroline (L-pyr) bridging ligand to a Co(II) metal centre by the environmental effect on the BF$_2$ capped dmgBF$_2$ ligand.[44] The acquisition of $^{59}$Co NMR spectra

of paramagnetic species with oxidation states of +2, +1, and 0 is very challenging, however, we have successfully acquired [59]Co NMR spectra of the chemically produced Co(I) species that resulted from the cobaloximes of complexes **1** and **2**. The quadrupolar nature of the cobalt nuclei (nuclear spin = 7/2) along with the paramagnetic nature of the +1 oxidation state results in very broad peaks (peak widths of several kHz) in the [59]Co NMR spectrum of Co(I) complexes.[86-89] When the complexes were reduced with 10 equivalents of [[n]Bu$_4$N]BH$_4$ in CD$_3$CN to give the Co(I) species, broad peaks with chemical shifts at 2996 ± 100 and 2443 ± 100 ppm were observed for complex **1** and complex **2**, respectively (Figure 10). When complex **1** was reduced with 10 equivalents of the reducing agent in the presence of five (5) equivalents of pyridine, a broad peak was observed at 2626 ± 100 ppm (Figure 10 and Table 4). Also the reduction of complex **1** by 10 equivalents of the reducing agent in the presence of five (5) equivalents of 2,3,5,6-tetrafluoropyridine in CD$_3$CN gave a broad peak resonating at 2499 ± 100 ppm (see ESI, Figure S46[†]). To the best of our knowledge, this represents the first report of the [59]Co NMR spectroscopy of the Co(I) species of the BF$_2$ capped cobaloxime in solution. The reduced form of the dmgBF$_2$ cobaloximes is reported in the literature as a pentacoordinate species with a square planar pyramidal geometry in the solid state.[27, 83] The presence of pyridine within the coordination sphere causes shielding in the [59]Co NMR spectra (Table 4 entries 5 and 6). There is a subtle difference in the symmetry of the broad peaks and the chemical shifts for the [Co(dmgBF$_2$)$_2$(py)]⁻ species generated from complex **2** and that of complex **1** in the presence of pyridine. This difference is most likely due to solvent effects (to which [59]Co NMR is very sensitive), where the solvent mixture in the latter case is made up of 2:98 % (v/v, py:CD$_3$CN) compared to the neat CD$_3$CN employed with complex **2**. Nevertheless, the chemical shift values are approximately equal when the uncertainty is considered. To truly characterize the Co(I) species of complex **1** in the presence and absence of pyridine and to circumvent the solvent effects, the acquisition of the spectra in the solid state will also be needed.

In our current study, ^{19}F and ^{11}B NMR spectra were also acquired in CD$_3$CN at ambient temperature for complexes **1** and **2** in the absence and presence of pyridine, 2,3,5,6-tetrafluoropyridine, and pentafluoropyridine, as well as solutions that were treated with excess [[n]Bu$_4$N]BH$_4$ to generate the corresponding Co(I) species. Studies of the Co(II) and Co(I) species of complexes **1** and **2** (see Table 4) corroborated the equilibrium and electrochemical studies. It must be noted that the ^{19}F NMR spectrum of complex **1** in acetonitrile-d$_3$ showed chemical shifts at −142.4, −150.1, −151.9, −168.4, and −189.2 ppm whereas in the ^{11}B NMR spectrum showed shifts at 41.18, 20.05, 3.00, and −1.14 (Table 4, entry 1). Like our electrochemical studies *vide supra*, the addition of five (5) equivalences of pyridine to complex **1** is expected to shift the equilibrium towards that of complex **2**. The coordination of pyridine (and its derivatives) is expected to reduce the number of conformations accessible to the BF$_2$ caps of the [dmgBF$_2$]⁻ ligands,[44] and consequently a reduction in the

number of resonances observed in the ^{19}F and ^{11}B NMR spectra of complex **2** (**Error! Reference source not found.**) compared to complex **1** in which the higher symmetry would allow for more conformers.

A mixture of complex **1** and five equivalences of pyridine gave three predominant peaks resonating at −147.3, −151.8, and −189.1 ppm in the ^{19}F NMR spectrum (see ESI, Figure S47[†]) and 43.95, 2.99, 2.54, 2.14, and −1.19 in the ^{11}B NMR spectrum. Comparing the spectrum of complex **2** dissolved in CD$_3$CN (Table 4, entry 2) with the mixture containing complex **1** and five equivalents of pyridine (Table 4, entry 3), it was evident that complex **2** dissociates to give complex **1** as shown in Eq. 1 above, as the ^{11}B and ^{19}F NMR spectra of complex **2** were equivalent to the additive spectra of complex **1** alone and complex **1** with five (5) equivalences of pyridine.
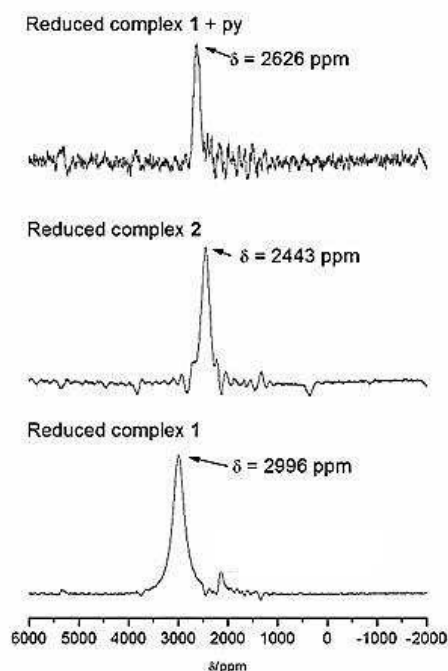


Figure 10. [59]Co NMR spectra of the Co(I) species produced from (i) 50 mM complex **1** and 500 mM [[n]Bu$_4$N]BH$_4$ (bottom), (ii) 50 mM complex **2** and 500 mM [[n]Bu$_4$N]BH$_4$ (middle), and (iii) 50 mM complex **1**, 250 mM pyridine, and 500mM [[n]Bu$_4$N]BH$_4$ (top). Solvent = CD$_3$CN.

Table 4. A summary of the NMR chemical shifts for [Co(dmgBF$_2$)$_2$(H$_2$O)$_2$] **1**, [Co(dmgBF$_2$)$_2$(H$_2$O)(py)]•0.5(CH$_3$)$_2$CO **2**, and the species formed upon reduction in CD$_3$CN.

| Entry | Species/mixture | $\delta_B$/ppm | $\delta_F$/ppm | $\delta_{Co}$/ppm[c] |
|---|---|---|---|---|
| 1 | Complex **1** | 41.18, 20.05, 3.00, −1.14 | −142.4, −150.1, −151.9, −168.4, −189.2 | -- |
| 2 | Complex **2** | 41.82, 19.68, 3.04-2.12 (m), 0.68 (t), −0.36 (d), −1.13 | −141.5, −142.4, −144.8, −147.7, −151.7, −154.9, −156.2, −188.9 | |
| 3 | Complex **1** + py | 43.95, 2.99, 2.54(d), 2.14, −1.19 | −147.3, −151.8, −189.1 | -- |
| 4 | Complex **1** + [$^n$Bu$_4$N]BH$_4$ | 19.48, 3.44, 3.35, 3.27, 0.76 (d) | −137.8, −138.3, −143.5, −150.8, −151.4 , −152.7 | 2996 |
| 5 | Complex **2** + [$^n$Bu$_4$N]BH$_4$ | 19.44, 3.19, 0.71 (d) | −139.1, −150.7, −151.4, −152.8 | 2443 |
| 6 | Complex **1** + [$^n$Bu$_4$N]BH$_4$ + py | 19.47, 3.11, 0.68 | −139.4, −150.4, −151.5, −152.9 | 2626 |
| 7 | Complex **1** + pyF$_5$ | 43.21, 2.93, −1.22 | −89.7, −134.9, −142.5, −150.3, −151.9, −162.7, −168.5, −189.1 | -- |
| 8 | Complex **1** + pyF$_4$ | 42.00, 20.02, 2.96, −1.18 | −78.3, −91.2, −93.9, −97.4, −138.4, −141.8, −144.0, −151.8, −165.8 | -- |
| 9 | pyF$_5$ (lit. [a]) [90, 91] | -- | −89.7 (−87.7), −134.8 (−134.3), −162.7 (−162.4) | -- |
| 10 | pyF$_4$ (lit. [a]) [90, 91] | -- | −92.6 (−92.6), −141.9 (−141.3) | -- |
| 11 | Complex **1** [b, 44] | 39.04, 3.55, 0.69 | −145.6 , −146.6, −148.4 | -- |

[a] tetrachloromethane
[b] DMSO-d$_6$
[c] uncertainty in the chemical shift, δ = ± 100 ppm.

The addition of 10 equivalences of the reducing [$^n$Bu$_4$N]BH$_4$ to the complexes to produce Co(I) species (Table 4, entries 4-6), resulted in the disappearance of the peak resonating at ~ −189 ppm in the $^{19}$F NMR spectra and the peak at ~ 41 ppm in the $^{11}$B NMR spectra in both complexes **1** and **2**. Also, in the $^{19}$F NMR spectra, the reduced form (a Co(I) species) of complex **1** had two additional peaks when compared to that of complex **2**, and a similar feature was observed with the Co(II) species. The reduction in the observed number of resonances point to a reduction in the number of conformations of the BF$_2$ capped dmgBF$_2$ ligand upon the coordination of pyridine (see Figure S46).[44] When complex **1** was reduced in the presence of five equivalences of pyridine (see ESI, Figure S49 c$^†$), a very similar spectrum to that of the reduced complex **2** was obtained, which further confirms the similarity of the species formed.

Polyfluorinated pyridines such as pentafluoropyridine (pyF$_5$) and 2,3,5,6-tetrafluoropyridine (pyF$_4$) should be very useful spectroscopic probes for $^{19}$F NMR measurements on pyridine coordinated to the cobalt(I) and cobalt(II) metal centres. The coordination of pyF$_5$ should result in changes in the chemical shifts of the *ortho-* and *para*-fluorine due to the inductive effect. The addition of five equivalences of pyF$_5$ to complex **1** did not result in noticeable changes in the $^{19}$F NMR spectrum. However, a mixture of pyF$_4$ and complex **1** showed new peaks in its $^{19}$F NMR spectrum which might be indicative of some coordination of the pyF$_4$. In this mixture (Table 4, entry 8), there is a downfield shift of the *ortho*-fluorine consistent with the coordination of the pyF$_4$ with a chemical shift at −97.4 ppm compared to the free pyF$_4$ at ca −93 ppm. There was no noticeable change in the $^{11}$B NMR of this mixture when compared to complex **1** only. These are consistent with our observations using UV-visible absorbance and cyclic voltammetry measurements (in acetonitrile or the ketone solvents (not shown)) in which no changes were observed with pyF$_5$ and miniscule changes with pyF$_4$. The pyF$_5$ species is initially defluorinated at the *para* position (to give 2,3,5,6-tetrafluoropyridine, pyF$_4$) in the presence of [Bu$_4$N]BH$_4$ (see ESI, Figure S50) and this type of reaction with a borohydride salt is well documented in the literature.[90, 91] A reaction between pyF$_4$ and [$^n$Bu$_4$N]BH$_4$ was also observed. Consequently, addition of 10 equivalents of the reducing agent, [$^n$Bu$_4$N]BH$_4$, to complex **1** along with five (5) equivalents of the pyF$_5$ or pyF$_4$ resulted in a plethora of peaks in the $^{19}$F NMR spectra of these mixtures (see ESI for example, Figure S51 and Table S7), which could not be unambiguously assigned to any species in solution. In the $^{11}$B NMR, we also observed numerous chemical shifts related to the various H$_{3-n}$BF$_n$ species formed subsequent to the defluorination reactions of the pyF$_5$ and/or pyF$_4$ species.[92, 93]

## Computational studies

The DFT-optimized geometries of complexes **1** and **2** in gas-phase and acetonitrile (using the IEF-PCM implicit solvation model) are in good agreement with the respective X-ray crystal structures[20, 83] (Figure 11). Each of these structures prefer a chair conformation of the macrocyclic ligand with aqua ligands forming a short H···F interaction (1.8-2.0 Å) to the nearest fluorine. Co-O distances in complex **1** are slightly longer than those found in the structure of [Co(dmgBF$_2$)$_2$(MeOH)$_2$]$^-$. For the reduced Co(I) species, the metal centre prefers five-coordination with a boat conformation of the (dmgBF$_2$)$_2$ ligand. Aqua ligands are too weak to coordinate to the Co(I) metal centre and dissociate to form hydrogen bonding interactions if optimizations were started from the six-coordinate complex. In [Co(dmgBF$_2$)$_2$(OH$_2$)]$^-$, hydrogen bonding of water to the Co(I) metal centre of the four-coordinate [Co(dmgBF$_2$)$_2$]$^-$ is slightly more stable than to the fluorides of the BF$_2$ bridging group. Similar square-planar complexes of Co(I) species with hydrogen bonding to the metal have been observed or proposed as intermediates in cobalamin or cobaloxime catalysis.[94-96] The boat and chair

conformations of the free $[Co(dmgBF_2)_2]^-$ complex are essentially degenerate and have $Co-N(dmgBF_2)$ bond distances similar to the five coordinate species. The optimized structure of $[Co(dmgBF_2)_2(py)]^-$ is in excellent agreement with the published structure[83] and the formation of this complex by displacement of water from $[Co(dmgBF_2)_2(H_2O)]^-$ is slightly favoured ($\Delta G$ = -1.3 kcal mol$^{-1}$) in acetonitrile. Attempts to optimize similar complexes with $pyF_4$ and $pyF_5$ resulted in dissociation to the four-coordinate complex. Acetonitrile is also less strongly coordinated to Co(I) in $[Co(dmgBF_2)_2(CH_3CN)]^-$ relative to the hydrogen-bonded four-coordinate complex ($\Delta G$ = +1.6 kcal mol$^{-1}$).
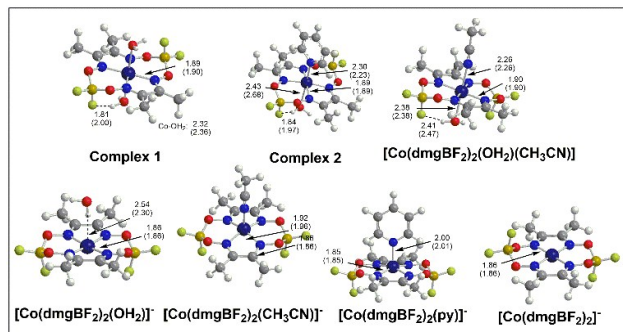


Figure 11. DFT-optimized geometries of complexes **1** and **2** in gas-phase and acetonitrile.

Comparison of the vertical TD-DFT excitation wavelengths and oscillator strengths ($f$) to the experimental spectra in Figure 8 suggests that these spectra are most consistent with the five-coordinate Co(I) species. Both $[Co(dmgBF_2)_2(py)]^-$ and $[Co(dmgBF_2)_2(CH_3CN)]^-$ have calculated transitions in the 530–620 nm region. The transitions for the $CH_3CN$ complex are similar in predicted intensity ($\lambda$ = 574 nm ($f$ = 0.03) and $\lambda$ = 538 nm ($f$ = 0.02)), but the longer wavelength excitation is more intense for the py complex ($\lambda$ = 613 nm ($f$ = 0.03) and $\lambda$ = 559 nm ($f$=0.02)). A third intense transition is found for each complex in the 400-500 range ($CH_3CN$: $\lambda$ = 420 nm and py: $\lambda$ = 478 nm). The four-coordinate $[Co(dmgBF_2)_2]^-$ is predicted to have a single significant transition in the visible region ($\lambda$ = 589 nm). These data appears to suggest five-coordination, but some contribution from four-coordinate Co(I) cannot be ruled out, especially in the case of water and the ketone solvents, where only one broad peak was observed for the Co(I) species which was formed from the reduction of complex **1** .

[59]Co NMR chemical shifts were calculated using DFT(mPW1PW91)-GIAO from the gas- and IEF-PCM-optimized structures of the Co(I/II) species and referenced to $[Co(CN)_6]^{3-}$ (Table 5). While the gas-phase shifts are within the range found experimentally, the IEF-PCM-derived values are found far outside of the range of the experimental NMR data, even when different implicit solvation methods are used. These results suggest that the implicit solvation method is not reliable for predicting [59]Co NMR chemical shifts, possibly due to the large negative charge on the reference. The [59]Co nucleus is known to be sensitive to the coordination geometry and molecular dynamics have been required to obtain

accurate chemical shifts in many cases.[97-99] For the Co(II) complexes, the gas-phase [59]Co shifts are within 500-600 ppm of the experimental values, within the error commonly found for DFT-GIAO studies of this nucleus.[100-103] The [59]Co NMR chemical shift of the complex with water hydrogen bonded to the Co(I) metal centre of $[Co(dmgBF_2)_2(H_2O)]^-$ is similar to the values found in the reduction of the Co(II), but the large differences between the results for complexes **1** ($\delta$ = 2996 ppm) and **2** ($\delta$ = 2443 ppm), suggest that different species are present in solution. The five coordinate py and $CH_3CN$ complexes have DFT-GIAO [59]Co chemical shifts that are much larger than the observed values, which may be attributed to an effect of large variations in the weak Co-L bond that calculations on static molecules cannot recover.[97-99] Taken together, the results of the TD-DFT calculations and DFT-GIAO chemical shifts cannot definitively assign the species observed experimentally, but suggest that the Co(I) complex is five-coordinate in the presence of py, but forms the $[Co(dmgBF_2)_2]^-$ ion when water and acetonitrile, are present as solvents.

Table 5. DFT(mPW1PW91)-GIAO [59]Co NMR chemical shifts[a] (ppm) of selected cobaloxime derivatives.

| Species | conformation | (gas phase) | ($CH_3CN$) |
|---|---|---|---|
| **1** | chair | 5775 | 8215 |
| **2** | chair | 5851 | 6961 |
| $[Co(dmgBF_2)_2(CH_3CN)(OH_2)]$ | chair | 5694 | 6477 |
| $[Co(dmgBF_2)_2py]^-$ | boat | 5430 | 6058 |
| $[Co(dmgBF_2)_2(CH_3CN)]^-$ | boat | 4186 | 5213 |
| $[Co(dmgBF_2)_2(OH_2)]^-$ | boat | 2343 | 2409 |
| $[Co(dmgBF_2)_2]^-$ | boat | 2418 | 2508 |
| $[Co(dmgBF_2)_2]^-$ | chair | 2212 | 2642 |

[a]calculated as $\delta^{iso} = ([ref.][[Co(CN)_6]^{3-}])^{iso} - (Co)^{iso}$

**Electrochemical behaviour of complexes 1 and 2 for the production of hydrogen in the presence of *p*-cyanoanilinium tetrafluoroborate in various solvents**

Complex **1** has been used as a benchmark for the activity of cobaloxime and other cobalt complexes employed in the electrocatalytic reduction of protons to form hydrogen, with a well-accepted mechanism (see Scheme S1).[19, 27] There is very little doubt that a Co(I) species is involved in the catalytic process. As such, a comparative study of complexes **1** and **2** under similar conditions was undertaken to determine if the pyridine influences the catalytic reduction of protons, and to simultaneously establish the effect of the relatively non-coordinating solvents on the apparent rate constant[27] for the electrocatalytic transformation. The overall rate constant for $H_2$ evolution was estimated from the height of the catalytic plateau current (Eq. 2).[27, 104]

$$i_c = nFA[cat]\sqrt{Dk_{app}[H^+]}$$

(2)

where the reaction rate constant, $k_{app}$ (M$^{-1}$ s$^{-1}$), can be estimated, where n is the number of electrons, $i_c$ is the plateau current (mA), F is the Faraday's constant (96485 C mol$^{-1}$), A is

the area of the electrode surface (cm$^2$), [cat] is the bulk concentration of the catalyst (M), $D$ is the diffusion coefficient (cm$^2$ s$^{-1}$), and [H$^+$] is the bulk concentration of acid (M). Controlled-potential electrolysis measurements for the production of hydrogen were conducted in a sealed two-chambered H-cell (see ESI, Figure S58[†]). These results are summarized in Table 6. The electrochemical behaviour of complexes **1** and **2** in acetonitrile gave an exact feature similar to what has been observed for complex **1** in the literature (see ESI, Figures S52-S54[†]).[27] Based on the amount of hydrogen produced, complex **1** performed better than complex **2** in acetonitrile, whereas this order was reversed in acetone. In 2-butanone, both complexes performed the same, within the margin of error, and were significantly less than acetone. To the best of our knowledge, this represents the first such study in ketone solvents. The trend in the $k_{app}$ and the turnover number (TON) for complex **1** *vs* complex **2**, suggests that in acetonitrile, there is a slight disadvantage to having the pyridine in the axial position, while in acetone it is advantageous. These variations support the proposition of the retention of the pyridine within the coordination sphere. Specifically, at the higher ratios of the acid source, if the pyridine was protonated and excluded from the coordination sphere, it would not significantly change the concentration of the *p*-cyanoanilium species, or alter the peak current and as such the production of hydrogen by both species would have been almost identical.

Table 6. Summary of data from electrocatalytic and controlled-potential electrolysis experiments.

| Entry | Solvent | Complex | $k_{app}$ / M$^{-1}$ s$^{-1}$ | Vol. H$_2$ / µL | TON (2 h) |
|-------|---------|---------|-------|-------|-----------|
| 1 | acetonitrile | **1** | 2068 ± 143 | 1140 ± 16 | 4.1 ± 0.2 |
| 2 | acetonitrile | **2** | 1571 ± 25 | 975 ± 34 | 3.5 ± 0.1 |
| 3 | acetone | **1** | 254 ± 21 | 299 ± 136 | 1.1 ± 0.5 |
| 4 | acetone | **2** | 183 ± 23 | 670 ± 49 | 2.3 ± 0.1 |
| 5 | 2-butanone | **1** | 177 ± 25 | 117 ± 29 | 0.4 ± 0.1 |
| 6 | 2-butanone | **2** | 123 ± 9 | 140 ± 26 | 0.5 ± 0.1 |

Controlled potential experiments are performed at 20 °C for 2 h on unstirred mixtures at a constant potential of −0.75 V in acetonitrile, −1.0 V in acetone and 2-butanone versus Ag, $n_{catalyst}$ = 12 mmol.

The results of the electrocatalytic reduction of the protons in these solvent systems have provided some clear conclusions. There is a linear correlation between the dielectric constant[105] of the non-aqueous solvent and the apparent rate constant for the reduction of the proton (see ESI, Figures S56 & S57[†]). This retardation points to the possible role of the solvent in stabilizing the transition states involved in the catalytic process, as the Co(I) species will be ionic, and ion-pairing is likely to retard the catalytic cycle. The presence of pyridine in the coordination sphere may enhance the performance of the catalyst based on the choice of the solvent. Owing to the fact that the presence of the pyridine in the coordination sphere generally shifts the Co$^{II/I}$ redox couple to a more positive value,

from a thermodynamic point of view, it was expected to enhance the performance of the catalyst as the proposed mechanism in the electrocatalytic reduction of protons by these species involves the formation of the Co(I) species. The structural effects induced by the solvent, and the electronic contribution from the pyridine may be strongly influential on the intricate mechanism (and the rate determining step) for the electrocatalytic reduction of protons, in comparison to the heterogeneous electron transfer to the complex, that can be deduced from the reduction potentials.

## Conclusions

This work has shown that the monopyridine species (complex **2**) is readily formed *in situ* upon the addition of pyridine and we are the first to successfully isolate this species. This monopyridine species exists in equilibrium with free pyridine and complex **1** in strongly coordinating solvents (acetonitrile and water), and the equilibrium is shifted towards the pyridine coordinated species in weakly coordinating solvents. The relative position of the equilibrium can be quickly determined by cyclic voltammetry and the absorption spectra. We have also successfully studied the Co(I)-pyridine interaction using $^{11}$B, $^{19}$F, $^{59}$Co NMR and UV-visible spectroscopy and the formation constant showed that the Co(I) species of the complex has a higher affinity for pyridine than Co(II) species. The data indicate that the presence of the pyridine in the coordination sphere influences the addition of an electron to the cobalt(I) oxidation state, irrespective of the solvent and suppresses the Co$^{I/0}$ reduction in the solvents explored. Importantly, the pyridine also slightly retards the rate constant for the reduction of protons supplied by *p*-cyanoanilinium tetrafluoroborate. These findings clearly indicate a solvent dependence and that the axial ligand influences the production of hydrogen, and may have implications in the design and performance of pyridine linked mixed-metal systems employing cobaloxime catalytic sites.

## Experimental

### Materials

Analytical or reagent grade chemicals obtained from commercial sources were used as received throughout this study. Microanalyses (C, H, B, Co, and N) were performed by the Microanalysis Laboratory at the University of Illinois Urbana/Champaign.

### Physical measurements

Magnetic susceptibility measurements were acquired on a Johnson Matthey® magnetic susceptibility balance, Mark I, at ambient temperature. All FTIR spectra were acquired in the range 4000-400 cm$^{-1}$ using the ATR accessory (with a diamond crystal) on a Nicolet 6700 FTIR spectrophotometer. $^{19}$F NMR spectra were acquired on a Bruker 400 MHz spectrometer with CD$_3$CN as solvent, with 50% CF$_3$CO$_2$H (δ = −76.55 ppm$^*$) used as an external reference at room temperature. $^{59}$Co NMR spectra

were acquired on a Bruker 400 MHz NMR using the Bruker "cpmg1d" pulse sequence for up to 120000 transients, and referenced to $K_3[Co(CN)_6]$[b] in acetonitrile-$d_3$ ($\delta$ = 293 ppm).[106] All NMR spectra were processed using Mestrec MNova software version 9.0. The first 20 to 40 data points of the time domain signal (FID) were corrected using backward linear prediction[107] in order to minimize spectral distortions due to probe ringing, with the fitting process employing either 128 or 256 data points. The Toeplitz method as implemented in the MNova program was used. After linear prediction, the FIDs were zero-filled to 256 K points and subjected to a Lorentzian exponential filter of 100 - 500 Hz prior to Fourier transformation.

All electrochemical experiments were performed at room temperature (ca 20 $^o$C) on a BASi® Epsilon C3 under an argon atmosphere in the respective solvents, thoroughly purged with Ar for 15 minutes before any electrochemical studies were carried out, and are uncorrected for junction potentials. A standard three electrode configuration was employed consisting of a glassy carbon working electrode (diameter = 3 mm), Pt wire auxiliary electrode and a Ag wire[‡] as reference electrode in non-aqueous solvents; against which the ferrocenium/ferrocene couple showed a reversible wave at +0.29 V in acetonitrile, +0.40 V in acetone, +0.55 V in 2-butanone, and +0.44 V in 1,2-difluorobenzene/acetone (4:1). In aqueous media, a AgCl/Ag reference electrode (BASi, 3.0 M NaCl) was employed, which was separated from the analytical solution by a Vicor® frit. The ionic strength was maintained at 0.10 M ([$^n$Bu$_4$N]ClO$_4$ in non-aqueous media and NaClO$_4$ in aqueous media).

Spectroelectrochemical measurements were regulated at 20 $^o$C with a thermostatic water bath/circulator (Thermo Scientific®). Absorbance measurements were performed on an Agilent® 8453A diode array spectrophotometer. A Pt gauze and Pt wire were employed as working and auxiliary electrodes, respectively, and Ag wire was used as a quasi-reference electrode. The ionic strength was maintained at 0.10 M as stated above. Each solution was purged with Ar for at least two minutes in the spectroelectrochemical cuvette (1 mm path length) prior to the measurement, and the spectra are acquired over 200–1000 s at a constant potential.

Electronic spectra were recorded on a Cary 5000 UV/Vis/NIR spectrophotometer, Spectramax M5 (Molecular Devices) or an Agilent 8453 diode array spectrophotometer in the respective solvent(s) using quartz cuvettes.

High-resolution ESI MS spectra were acquired via positive electrospray ionization on a Bruker 12 Tesla APEX –Qe FTICR-MS with an Apollo II ion source. Samples were dissolved in 1:1 dichloromethane/methanol, followed by direct injection using a syringe pump with a flow rate of 2 $\mu$L s$^{-1}$. The data was processed using Bruker Daltonics Data Analysis Version 3.4.

Controlled-potential electrolysis measurements for the production of hydrogen were conducted on unstirred solutions for two hours in a sealed two-chambered H-cell separated by a fine frit, where one chamber held the working and reference electrodes in 10 mL of 1 mM of complex in 0.10 M [$^n$BuN$_4$]ClO$_4$ (supporting electrolyte) with 0.4 M p-cyanoanillinium (proton

source) and the second chamber held the auxiliary electrode in 5 mL of the solvent with the supporting electrolyte. A glassy carbon plate (contact area ~2 cm × 1 cm × 3 mm) and Pt wire were used as the working and auxiliary electrodes, respectively, with Ag wire as the reference electrode. The solution was purged with Ar for 20 minutes and then sealed under an Ar atmosphere before the start of each electrolysis experiment. The amount of $H_2$ evolved was quantified from an analysis of the headspace of the chamber containing the working electrode with a Shimadzu Tracera gas chromatograph 2010 Plus (SH-Rt-Molsieve 30 m × 0.53 mm × 50 $\mu$m column; 40 $^o$C isothermal; 1.0 mL min$^{-1}$ flow rate; He carrier gas, 50 $\mu$L injection volume) using a barrier-discharge ionization detector (BID). A calibration of hydrogen was performed by injecting known amounts of hydrogen gas into an airtight vial of the same volume as the reaction vessel and filled with solvent (10 mL) to account for the fraction that dissolves in the solvent. The turn-over-number (TON) is calculated from $n_{H_2}/n_{cat}$, where $H_2$ is assumed to behave as an ideal gas at the low pressures of the experiment.

### DFT calculations

Geometries were optimized in the gas- and solution-phase using Gaussian 09[§] with the DFT-mPW1PW91[108] functional and the integral equation formalism variant of the polarisable continuum mode (IEF-PCM) implicit solvation method.[109] Cobalt was represented by the Wachters-Hay all-electron basis set.[110, 111] The Dunning triple-$\zeta$ basis set augmented with diffuse and polarization functions was for all other atoms.[112] Vertical transitions were calculated using time-dependent DFT (TD-DFT) from the optimized geometry. $^{59}$Co NMR chemical shifts were calculated relative to $K_3[Co(CN)_6]$ at the gas- or IEF-PCM-optimized geometry. Optimized structures were confirmed as minima on the potential energy surface by vibrational analysis.

### Synthesis of [Co(dmgBF$_2$)$_2$(H$_2$O)$_2$] 1

[Co(dmgBF$_2$)$_2$(H$_2$O)$_2$] **1** was synthesized using the methods of Bakac *et al.*[20] The measured $\mu_{eff}$ = 1.84 B.M. compared favourably to the literature value of 1.92 B.M.[20] The spectral characteristics of complex **1** in the UV-visible-NIR region with acetonitrile solvent have been thoroughly documented in the literature.[44]

### Synthesis of [Co(dmgBF$_2$)$_2$(H$_2$O)(py)]●0.5CH$_3$COCH$_3$ 2

[Co(dmgBF$_2$)$_2$(H$_2$O)$_2$] (0.30 g, 0.71 mmol), along with pyridine (79 mg, 1.0 mmol) and acetone (400 mL) were mixed in a 500 mL RB flask; then the reaction mixture was stirred at room temperature for 21.5 hours. The reaction mixture was rotary evaporated to dryness; and more acetone was added to the mixture. The mixture was once more rotary evaporated, and the resulting solid was washed with diethyl ether and a dry solid was recovered. Yield = 0.33 g (89%). Anal. Calcd. for $C_{14.5}H_{22}B_2CoF_4N_5O_{5.5}$: C, 34.09; H, 4.34; B, 4.23; Co, 11.53; N, 13.71. Found: C, 33.79; H, 3.71; B, 4.48; Co, 11.71; N, 13.79. High-resolution ESI MS (positive mode) *m/z* = of 482.083653

for the $[Co(dmgBF_2)_2(H_2O)(py)]^+$ species. $\mu_{eff}$ = 1.28 ± 0.02 B.M. Selected $\nu_{max}$ / cm$^{-1}$: 537.6 (s) (Co-N(O-B)), 689.8 (m) (py), 758.3 (m) (py), 822.8 (vs) (B-F), 1100.8 (s) (N-O), 1163.5 (s) (B-F), 1225.1 (m) (N-O), and 1622.0 (m) (C=N). UV-visible spectrum (CH$_3$CN), $\lambda_{max.}$/nm ($10^{-3}$ $\varepsilon$/M$^{-1}$ cm$^{-1}$): 199 (47.6), 256 sh (15.0), 323 sh (4.1), 425 (4.8), and 1144 (0.15).

**Mole ratio studies and calculation of equilibrium constants with complex 1.**

Spectrophotometric titrations were carried on solutions of complex **1** in various solvents, viz., acetonitrile, acetone, 2-butanone, dichloromethane, and 1,2-difluorobenzene/acetone (4:1, v/v) (0.10 mM for UV-visible spectroscopy and 2.0 mM for NIR spectroscopy), with the concentration of pyridine varying as 0.00 mM ≤ [pyridine] ≤ 10.00 mM. The solutions in 10 mL volumetric flasks were equilibrated at 20 $^o$C; then their absorbances were acquired after 10 minutes and again after 24 hours. The stoichiometry and values of the equilibrium constant were determined from the absorbance data, the slope and intercept of an appropriate plot (Eq. 1 and see ESI), using an established equation as reported in the literature as shown in Eq. 3.[22, 76]

$$\log_{10}\left(\frac{A_0 - A_{eq}}{A_{eq} - A_\infty}\right) = \log K + n \log[\text{pyridine}]$$

(3)

In Eq. 3, $A_{eq}$ = equilibrium absorbance at 1162 nm ($\lambda_{max}$) for acetonitrile, 372 nm ($\lambda_{min}$) for acetone, and 2-butanone, and 370 nm for dichloromethane; $A_0$ = absorbance before the addition of pyridine and $A_\infty$ = theoretical absorbance for the infinite addition of pyridine. $A_\infty$ is estimated from the limiting value predicted from the mole ratio plot:

$$[\text{pyridine}] = [\text{pyridine}]_T - \left(\frac{A_0 - A_{eq}}{A_0 - A_\infty}\right)[M]$$

(4)

where [pyridine]$_T$ and [M] denote the total concentrations of pyridine and the metal complex, respectively.

Spectrophotometric titrations involving a Co(I) species (which was generated from the reaction between complex **1** (1.0 mM) and [$^n$BuN$_4$]BH$_4$ (500 equivalents) and the required aliquots of pyridine (0 mM ≤ [pyridine] ≤ 4.0 mM)) were performed in acetonitrile under a blanket of argon in a cuvette (1 mm path length) until a limiting UV-visible spectrum was acquired; A$_{eq}$ in Eq. 3&4 = 447 nm.

1. R. Eisenberg and D. G. Nocera, *Inorg. Chem.*, 2005, **44**, 6799-6801.
2. H. B. Gray, *Nature Chemistry*, 2009, **1**, 112.
3. W. Lubitz and W. Tumas, *Chem. Rev.*, 2007, **107**, 3900-3903.
4. R. F. Service, *Science*, 2005, **309**, 548-551.
5. J. M. Lehn and J. P. Sauvage, *Nouv. J. Chim.*, 1977, **1**, 449–451.

## Notes and references

‡ Footnotes relating to the main text should appear here. These might include comments relevant to but not central to the matter under discussion, limited experimental and spectral data, and crystallographic data.
§
§§
etc.
* http://chemnmr.colorado.edu/manuals/19F_NMR_Reference_Standards.pdf
ƚ) 0.1 M K$_3$[Co(CN)$_6$] with 3.5 equivalents of 18-crown-6 ether to aid with dissolution.
‡ Ag wire serves as a convenient reference across the multiple solvents and simultaneously eliminates the junction potential that will develop across the frit of the AgCl/Ag aqueous reference electrode. The performance of the Ag wire was compared to AgCl/Ag reference with the acetonitrile solutions where it was found to give equivalent cyclic voltammograms, and the behaviour of the Ag quasi-reference electrode was reproducible across several days of experiments.
§ Gaussian 09, Gaussian, Inc., Wallingford, CT, 2009.

6. A. T. Ashcroft, A. K. Cheetham, J. S. Foord, M. L. H. Green, C. P. Grey, A. J. Murrell and P. D. F. Vernon, *Nature*, 1990, **344**, 319-321.
7. M. Kobayashi, S. Masaoka and K. Sakai, *Angew. Chem. Int. Ed.*, 2012, **51**, 7431-7434.
8. G. Singh Bindra, M. Schulz, A. Paul, R. Groarke, S. Soman, J. L. Inglis, W. R. Browne, M. G. Pfeffer, S. Rau, B. J. MacLean, M. T. Pryce and J. G. Vos, *Dalton Trans.*, 2012, **41**, 13050-13059.
9. W. T. Eckenhoff and R. Eisenberg, *Dalton Trans.*, 2012, **41**, 13004-13021.

10. R. B. Gordon, M. Bertram and T. E. Graedel, *Proc. Natl. Acad. Sci. USA*, 2006, **103**, 1209-1214.

11. J. L. Dempsey, B. S. Brunschwig, J. R. Winkler and H. B. Gray, *Acc. Chem. Res.*, 2009, **42**, 1995-2004.

12. P. Du, K. Knowles and R. Eisenberg, *J. Am. Chem. Soc.*, 2008, **130**, 12576-12577.

13. P. Du, J. Schneider, G. Luo, W. W. Brennessel and R. Eisenberg, *Inorganic Chemistry* 2009, **48**, 4952-4962.

14. A. Fihri, V. Artero, M. Razavet, C. Baffert, W. Leibl and M. Fontecave, *Angew. Chem. Int. Ed.* , 2008, **47**, 564-567.

15. M. Bacchi, G. Berggren, J. Niklas, E. Veinberg, M. W. Mara, M. L. Shelby, O. G. Poluektov, L. X. Chen, D. M. Tiede, C. Cavazza, M. J. Field, M. Fontecave and V. Artero, *Inorg. Chem.*, 2014, **53**, 8071-8082.

16. M. Razavet, V. Artero and M. Fontecave, *Inorg. Chem.*, 2005, **44**, 4786-4795.

17. J. L. Dempsey, J. R. Winkler and H. B. Gray, *J. Am. Chem. Soc.*, 2010 **132**, 1060–1065.

18. A. Han, H. Wu, Z. Sun, H. Jia, Z. Yan, H. Ma, X. Liu and P. Du, *ACS Applied Materials & Interfaces*, 2014, **6**, 10929-10934.

19. C. N. Valdez, J. L. Dempsey, B. S. Brunschwig, J. R. Winkler and H. B. Gray, *Proc. Natl. Acad. Sci. USA*, 2012, **109**, 15589–15593.

20. A. Bakac, M. E. Brynildson and J. H. Espenson, *Inorg. Chem.*, 1986, **25**, 4108-4114.

21. A. Bakac and J. H. Espenson, *J. Am. Chem. Soc.*, 1984, **106**, 5197-5202.

22. Y. Nonaka and K. Hamada, *Bull. Chem. Soc. Jpn.*, 1981, **54**, 3185-3190.

23. G. N. Schrauzer and R. J. Windgassen, *J. Am. Chem. Soc.*, 1966, **88**, 3738-3743.

24. K. Wang and R. B. Jordan, *Can. J. Chem.*, 1996, **74**, 658-665.

25. R. M. Kellett and T. G. Spiro, *Inorg. Chem.*, 1985, **24**, 2373-2377.

26. B. J. Fisher and R. Eisenberg, *J. Am. Chem. Soc.*, 1980, **102**, 7361-7363.

27. X. Hu, B. S. Brunschwig and J. C. Peters, *J. Am. Chem. Soc.*, 2007, **129**, 8988-8998.

28. P. A. Jacques, V. Artero, J. Pecaut and M. Fontecave, *Proc. Natl. Acad. Sci. USA*, 2009, **106**, 20627-20632.

29. C. Creutz, H. A. Schwarz and N. Sutin, *J. Am. Chem. Soc.*, 1984, **106**, 3036-3037.

30. H. Schwarz, C. Creutz and N. Sutin, *Inorg. Chem.*, 1985, **24**, 433-439.

31. W. M. Singh, T. Baine, S. Kudo, S. Tian, X. A. N. Ma, H. Zhou, N. J. DeYonker, T. C. Pham, J. C. Bollinger, D. L. Baker, B. Yan, C. E. Webster and X. Zhao, *Angew. Chem. Int. Ed.*, 2012, **51**, 5941-5944.

32. Y. Sun, J. P. Bigi, N. A. Piro, M. L. Tang, J. R. Long and C. J. Chang, *J. Am. Chem. Soc.*, 2011, **133**, 9212-9215.

33. M. Vennampalli, G. Liang, L. Katta, C. E. Webster and X. Zhao, *Inorg. Chem.*, 2014, **53**, 10094-10100.

34. B. D. Stubbert, J. C. Peters and H. B. Gray, *J. Am. Chem. Soc.*, 2011, **133**, 18070-18073.

35. P. Zhang, P.-A. Jacques, M. Chavarot-Kerlidou, M. Wang, L. Sun, M. Fontecave and V. Artero, *Inorg. Chem.*, 2012, **51**, 2115-2120.

36. W. R. McNamara, Z. Han, C.-J. Yin, W. W. Brennessel, P. L. Hollan and R. Eisenberg, *Proc. Natl. Acad. Sci. USA*, 2012, **109**, 15594–15599.

37. S. M. Laga, J. D. Blakemore, L. M. Henling, B. S. Brunschwig and H. B. Gray, *Inorg. Chem.*, 2014, **53**, 12668-12670.

38. M. Shamsipur, A. Salimi, H. Haddadzadeh and M. F. Mousavi, *J. Electroanal. Chem.*, 2001, **517**, 37-44.

39. D. W. Wakerley and E. Reisner, *Phys. Chem. Chem. Phys.*, 2014, **16**, 5739-5746.

40. S. C. Marinescu, J. R. Winkler and H. B. Gray, *Proc. Natl. Acad. Sci. USA*, 2012, **109**, 15127-15131.

41. G. Smolentsev, A. A. Guda, M. Janousch, C. Frieh, G. Jud, F. Zamponi, M. Chavarot-Kerlidou, V. Artero, J. A. van Bokhoven and M. Nachtegaal, *Faraday Discuss.*, 2014, **171**, 259-273.

42. J. Krzystek, A. Ozarowski, S. A. Zvyagin and J. Telser, *Inorg. Chem.*, 2012, **51**, 4954-4964.

43. J. C. Manton, C. Long, J. G. Vos and M. T. Pryce, *Dalton Trans.*, 2014, **43**, 3576-3583.

44. D. M. Cropek, A. Metz, A. M. Muller, H. B. Gray, T. Horne, D. C. Horton, O. Poluektov, D. M. Tiede, R. T. Weber, W. L. Jarrett, J. D. Phillips and A. A. Holder, *Dalton Trans.*, 2012, **41**, 13060-13073.

45. A. Fihri, V. Artero, A. Pereira and M. Fontecave, *Dalton Trans.*, 2008, 5567-5569.

46. A. Kahnt, K. Peuntinger, C. Dammann, T. Drewello, R. Hermann, S. Naumov, B. Abel and D. M. Guldi, *J. Phys. Chem. A*, 2014, **118**, 4382-4391.

47. V. A. Kawade, S. Ghosh, A. V. Sapre and A. S. Kumbhar, *J. Chem. Sci.*, 2010, **122**, 225-232.

48. C. Ducker-Benfer, M. S. A. Hamza, C. Eckhardt and R. Van Eldik, *Eur. J. Inorg. Chem.*, 2000, 1563-1569.

49. A. M. Funston, W. D. McFadyen and P. A. Tregloan, *J. Chem. Soc. Dalton Trans.*, 2002, 2053-2060.

50. M. Kumar, E. Natarajan and P. Neta, *J. Phys. Chem.* , 1994, **98**, 8024-8029.

51. V. A. Kawade, A. S. Kumbhar, D. B. Naik and R. J. Butcher, *Dalton Trans.*, 2010, **39**, 5664-5675.

52. Q. G. Mulazzani, S. Emmi, P. G. Fuochi, M. Venturi, M. Z. Hoffman and M. G. Simic, *J. Phys. Chem.*, 1979, **83**, 1582-1590.

53. M. Simic and M. Ebert, *Int. J. Radiat. Phys. Chem.*, 1971, **3**, 259-272.

54. L. Helm and A. E. Merbach, *Chem. Rev.*, 2005, **105**, 1923-1960.

55. K. Wang and R. B. Jordan, *Inorg. Chem.*, 1995, **34**, 5672-5679.

56. A. Bakac and J. H. Espenson, *J. Am. Chem. Soc.*, 1984, **106**, 5197-5202.

57. C. C. L. McCrory, C. Uyeda and J. C. Peters, *J. Am. Chem. Soc.*, 2012, **134**, 3164-3170.

58. P. Zhang, M. Wang, J. Dong, X. Li, F. Wang, L. Wu and L. Sun, *J. Phys. Chem. C*, 2010, **114**, 15868-15874.

59. M. Razavet, V. Artero and M. Fontecave, *Inorg. Chem.*, 2005, **44**, 4786-4795.

60. P. Du, J. Schneider, G. Luo, W. W. Brennessel and R. Eisenberg, *Inorg. Chem.*, 2009, **48**, 4952-4962.

61. A. Rockenbauer, E. Budo-Zahonyi and L. I. Simandi, *J. Chem. Soc., Dalton Trans.*, 1975, 1729-1737.

62. V. Artero, M. Chavarot-Kerlidou and M. Fontecave, *Angew. Chem. Int. Ed.*, 2011, **50**, 7238-7266.

63. S. Varma, C. E. Castillo, T. Stoll, J. Fortage, A. G. Blackman, F. Molton, A. Deronzier and M. N. Collomb, *Phys. Chem. Chem. Phys.*, 2013, **15**, 17544-17552.

64. A. A. Holder and T. P. Dasgupta, *Inorg. Chim. Acta*, 2002, **331**, 279-289.

65. A. A. Holder, T. P. Dasgupta and S.-C. Im, *Transition Met. Chem.*, 1997, **22**, 135-140.

66. A. A. Holder and T. P. Dasgupta, *J. Chem. Soc. Dalton Trans.*, 1996, 2637-2643.

67. A. A. Holder, T. P. Dasgupta, W. McFarlane, N. H. Rees, J. H. Enemark, A. Pacheco and K. Christensen, *Inorg. Chim. Acta*, 1997, **260**, 225-228.

68. L. M. Moody, S. Balof, S. Smith, V. H. Rambaran, D. VanDerveer and A. A. Holder, *Acta Crystallogr. Sect. E: Struct. Rep. Online*, 2008, **E64**, m262-m263.

69. V. H. Rambaran, T. R. Erves, K. Grover, S. Balof, L. V. Moody, S. E. Ramsdale, L. A. Seymour, D. VanDerveer, D. M. Cropek, R. T. Weber and A. A. Holder, *J Chem Crystallogr*, 2013, **43**, 509-516.

70. H. Yuan, D. A. L. Newton, L. A. Seymour, A. Metz, D. Cropek, A. A. Holder and R. Y. Ofoli, *Catal. Commun.*, 2014, **56**, 76-80.

71. M. A. W. Lawrence, C. D. McMillen, R. K. Gurung, M. J. Celestine, J. F. Arca and A. A. Holder, *J Chem Crystallogr*, 2015, **45**, 427-433.

72. J. E. Varey, G. J. Lamprecht, V. P. Fedin, A. Holder, W. Clegg, M. R. J. Elsegood and A. G. Sykes, *Inorg. Chem.*, 1996, **35**, 5525-5530.

73. A. A. Holder, R. F. G. Brown, S. C. Marshall, V. C. R. Payne, M. D. Cozier, W. A. Alleyne and C. O. Bovell, *Transition Met. Chem.*, 2000, **25**, 605-611.

74. M. A. W. Lawrence and A. A. Holder, *Inorg. Chim. Acta*, 2016, **441**, 157-168.

75. N. Yamazaki and Y. Hohokabe, *Bull. Chem. Soc. Jpn.*, 1971, **44**, 63-69.

76. S. L. Vilakazi and T. Nyokong, *Polyhedron*, 1998, **17**, 4415-4423.

77. C. Baffert, V. Artero and M. Fontecave, *Inorg. Chem.*, 2007, **46**, 1817-1824.

78. K.-A. Green, P. T. Maragh, K. Abdur-Rashid, A. J. Lough and T. P. Dasgupta, *Eur. J. Inorg. Chem.*, 2014, **2014**, 3600-3607.

79. I. Larrosa, C. Somoza, A. Banquy and S. M. Goldup, *Org. Lett.*, 2011, **13**, 146-149.

80. M. G. Organ, M. Abdel-Hadi, S. Avola, N. Hadei, J. Nasielski, J. O'Brien C and C. Valente, *Chem. Eur. J.*, 2007, **13**, 150-157.

81. C. Valente, M. E. Belowich, N. Hadei and M. G. Organ, *Eur. J. Org. Chem.*, 2010, 4343–4354.

82. O. Pantani, E. Anxolabéhère-Mallart, A. Aukauloo and P. Millet, *Electrochem. Commun.*, 2007, **9**, 54-58.

83. S. Shi, L. M. Daniels and J. H. Espenson, *Inorg. Chem.*, 1991, **30**, 3407-3410.

84. O. M. Williams, A. H. Cowley and M. J. Rose, *Dalton Trans.*, 2015, **44**, 13017-13029.

85. W. von Philipsborn, *Chem. Soc. Rev.* , 1999, **28**, 95-105.

86. R. Benn, K. Cibura, P. Hofmann, K. Jonas and A. Rufinska, *Organometallics*, 1985, **4**, 2214-2221.

87. E. A. C. Lucken, K. Noack and D. F. Williams, *J. Chem. Soc. A*, 1967, 148-154.

88. A. Medek, V. Frydman and L. Frydman, *Proc. Natl. Acad. Sci. USA*, 1997, **94**, 14237-14242.

89. C. Sizun, P. Kempgens, J. Raya, K. Elbayed, P. Granger and J. Rosé, *J. Organomet. Chem.*, 2000, **604**, 27-33.

90. C. Bobbio, T. Rausis and M. Schlosser, *Chem. Eur. J.*, 2005, **11**, 1903-1910.

91. P. L. Coe, A. G. Holton and J. C. Tatlow, *J. Fluorine Chem.*, 1982, **21**, 171-189.

92. T. C. Farrar and T. D. Coyle, *J. Chem. Phys.*, 1964, **41**, 2612-2613.

93. C. W. Heitsch, *Inorg. Chem.*, 1965, **4**, 1019-1024.

94. T. C. Moore, S. A. Newmister, I. Rayment and J. C. Escalante-Semerena, *Biochemistry*, 2012, **51**, 9647-9657.

95. M. Kumar, N. Kumar, H. Hirao and P. M. Kozlowski, *Inorg. Chem.*, 2012, **51**, 5533-5538.

96. B. H. Solis and S. Hammes-Schiffer, *Inorg. Chem.*, 2011, **50**, 11252-11262.

97. C. Kritayakornupong, K. Plankensteiner and B. M. Rode, *J. Chem. Phys.*, 2003, **119**, 6068-6072.

98. M. Bühl, S. Grigoleit, H. Kabrede and F. T. Mauschick, *Chem. Eur. J.*, 2006, **12**, 477-488.

99. S. Grigoleit and M. Bühl, *J. Chem. Theory Comput.*, 2005, **1**, 181-193.

100. J. C. C. Chan, S. C. F. Au-Yeung, P. J. Wilson and G. A. Webb, *J. Mol. Struct. THEOCHEM*, 1996, **365**, 125-130.

101. J. C. C. Chan and S. C. F. Au-Yeung, *J. Mol. Struct. THEOCHEM*, 1997, **393**, 93-96.

102. J. C. C. Chan and S. C. F. Au-Yeung, *J. Phys. Chem. A*, 1997, **101**, 3637-3640.

103. N. Godbout and E. Oldfield, *J. Am. Chem. Soc.*, 1997, **119**, 8065-8069.

104. J.-M. Savéant, *Chem. Rev.*, 2008, **108**, 2348-2378.

105. *CRC Handbook of Chemistry and Physics*, CRC Press LLC, 82 edn., 2001.

106. T. Taura, *Bull. Chem. Soc. Jpn.*, 1990, **63**, 1105-1110.

107. P. Koehl, *Prog. Nucl. Magn. Reson. Spectrosc.*, 1999, **34**, 257-299.

108. C. Adamo and V. Barone, *J. Chem. Phys.*, 1998, **108**, 664-675.

109. J. Tomasi, B. Mennucci and R. Cammi, *Chem. Rev.*, 2005, **105**, 2999–3094.

110. P. J. Hay, *J. Chem. Phys.*, 1977, **66**, 4377-4384.

111. A. J. H. Wachters, *J. Chem. Phys.*, 1970, **52**, 1033-1036.

112. T. H. Dunning, *J. Chem. Phys.*, 1971, **55**, 716-723.

Computational, electrochemical, and spectroscopic studies of two mononuclear cobaloximes with and without an axial pyridine were investigated to identify Co(I) and Co(II) species